Research article Available online www.ijsrr.org ISSN: 2279–0543

International Journal of Scientific Research and Reviews

Morphological Properties of Titanium-Niobium Alloys with Different Compositions on Glass Substrate

Aditi[1*] and Tyagi Anand K.[2]

[1]Department of Applied Sciences, I. K. Gujral Punjab Technical University, Jalandhar (Punjab), India Email - aditigoyal2210@gmail.com
[2]Department of Applied Sciences, SBS State Technical Camus, Firozpur (Punjab), India

ABSTRACT

In the present study, thin films of Titanium-Niobium alloy were deposited on glass substrates by Radio-Frequency (RF) Magnetron Sputtering under sputtering power 100W at a relatively low temperature (200 ºC). The films were characterized for structure, morphology and microstructure properties by using X-ray Diffraction (XRD), Field Emission Scanning Electron Microscopy (FESEM) and Atomic Force Microscopy (AFM). Thin films with five different compositions;$Ti_{90}Nb_{10}$ (Ti-17.7 wt.% Nb), $Ti_{80}Nb_{20}$ (Ti-33 wt.% Nb), $Ti_{70}Nb_{30}$ (Ti-45 wt.% Nb), $Ti_{60}Nb_{40}$ (Ti-56 wt.% Nb) and $Ti_{50}Nb_{50}$ (Ti-66 wt.% Nb)) were prepared. XRD results exhibited only single prominent peak corresponding to Ti-Nb (110) orientation of hexagonal close packed structure. With the increase in Nb content, the grain size of Ti-Nb alloy films increases and hence surface roughness of this alloy decreases with increase of Niobium content.

KEYWORDS: Ti-Nb alloy, RF Sputtering, Microstructure, Morphological Properties

***Corresponding author**

Aditi

Department of Applied Sciences,

I. K. Gujral Punjab Technical University,

Jalandhar (Punjab), India.

Email - aditigoyal2210@gmail.com

INTRODUCTION:

Titanium and its alloys have been used in many engineering applications covering a variety of areas, such as aerospace, marine, biomaterials, chemical industries, sports, etc due to their unique combination of outstanding mechanical and chemical properties. With the increasing content of niobium, an improvement in the toughness, strength, formability and weldability of the alloy has been observed, making it suitable for aerospace, medical, and industrial applications. [1,2] As niobium is hypoallergenic, it is especially suitable for use in titanium medical implants. It also helps in fabrication of fine grained Titanium-Niobium based super alloys with controlled density and microstructure that lends itself well for jet engine components. The properties Ti-Nb alloys depend critically on the chemical composition and phase stabilization.[3] The pure titanium crystallizes in either a hexagonal close-packed crystalline structure, called the alpha (α) phase below 882°C, or a body-centered cubic structure, called the beta (β) phase above 882°C. β-type titanium alloys have the lowest modulus due to the low density of the Body-Centered Cubic (BCC) structure.[4] Alloying the different elements with pure Ti provides an efficient clue for organizing the Ti atoms in either of these two allotropic forms. Commonly, a blend of two forms wherein both α and β coexist is used in most of the applications. The relative contents of two phases and microstructure of this alloy finally decide its properties.

In a number of recent studies, α and β-phases have been detected to coexist in Ti-Nb alloy system.[5,6] However, there are no research reports on investigations on properties of Ti-Nb alloys for full range of composition. A systematic investigation and quantification of the influence of composition Ti-xNb alloys (x = 10, 20, 30,40 and 50 at%) on the microstructural features of Titanium-niobium thin films are essential for tailoring out its properties like strength, roughness and adhesion in biomedical and microelectronics applications. Owing to these facts, the present work has been focused on to deposit Titanium-Niobium films on glass substrate by RF Magnetron Sputtering and to characterize them mainly for their microstructural evolution features by XRD, FESEM, and AFM. What would be the effect of increase in niobium in Ti-Nb alloy on the texture, roughness and grain size of Ti-Nb films has been investigated in the present work.

EXPERIMENTAL DETAILS:

Deposition:

The Ti-Nb films were deposited by RF magnetron sputtering onto glass substrates using Titanium- Niobium alloy target (50-mm diameter and 3-mm thick) with a minimum purity of 99.9%.

The glass substrates were cleaned by rinsing in ultrasonic baths of acetone for 10-15 minutes and dried. Glass substrates were cut into different sizes of requirement and clamped on the substrate holder in the chamber. Vacuum was created in the sputtering chamber not less than 10^{-6} Torr by using a turbo molecular pump. Commercial argon (Ar) gas of 99.9% purity was used as the sputtering gas and it has kept constant at gas flow rate of 15 sccm that can be controlled by a mass flow controller. Base pressure was kept at $8x10^{-6}$ mbar and working pressure was 1.7 x 10^{-2} mbar. In this process target-substrate distance was kept at 7-8 cm. Sputtering RF power and substrate temperature were kept constant at 100W and 200°C respectively. The deposition times of the films with different compositions of the alloy were selected so as to deposit the same thickness of 200 nm. Table 1 below lists out the deposition times for various compositions. It is clear that as the Nb content increases deposition time decreases. In sample/target Ti90Nb10 a deposition rate of 0.2 to 0.3 Å/s was observed, however, in case of sample/target Ti50Ni50, the deposition rate was found to be much faster around 0.4-0.6 Å/s.

Table-1: Deposition time of thin films on substrate

Sample/Target Composition	Ti90Nb10	Ti80Nb20	Ti70Nb30	Ti60Nb40	Ti50Nb50
Deposition Time (min)	118	104	93	64	59

Characterization:

The phases were analyzed by X-Ray Diffractometer (Panalytical X Pert Pro) at 40 kV and 30 mA using a Ni-filtered with Cu K_α (λ = 1.54056 Å) radiation source. The scanning speed was 2°/min and the scanning angle 2θ ranged from 10° to 80°. Phases were identified by matching their characteristic peaks with files of the Joint Committee on Powder Diffraction Standards (JCPDS). The surface topographical characterizations of the Ti films were obtained from FESEM (Nova Nano Fe-SEM 450) (FEI). It provides ultra high resolution characterization & analysis giving precise, true nanometer scale information. It gives a resolution of 1.4 nm at 1 kV (TLD-SE) & 1 nm at 15 kV (TLD-SE). We have done EDX attached with SEM for measuring the elemental chemical composition of materials. Beam landing energy can go down from 30 keV to 50 eV. The surface morphology (AFM) of the Ti films was also characterized by using Multimode Scanning Probe Microscope (Bruker).

RESULTS AND DISCUSSION:

Fig. 1 shows the XRD patterns for Ti-Nb alloy thin films deposited on glass substrate at 200°C, showing (110), (101), (200), (112) and (112) diffraction peaks that are characteristics of α and β titanium phases. The phases were identified by matching each characteristic peak with the JCPDS files (JCPDS

card No.44-1294). [7,8] For Ti90Nb10 alloy, the main phase constituent is α phase. When Nb content increases, α phase peak diminished gradually. The XRD patterns clearly indicate the coexistence of α and β phases. The peaks at positions 2θ (42.29°, 73.50°, 77.20°) are related to α- Ti phase and those present at 36.31° and 61.1° correspond to β- Ti phases. The peaks corresponding to α- Ti phase are found to be considerably weakened and diminished at the sample Ti80Nb20.

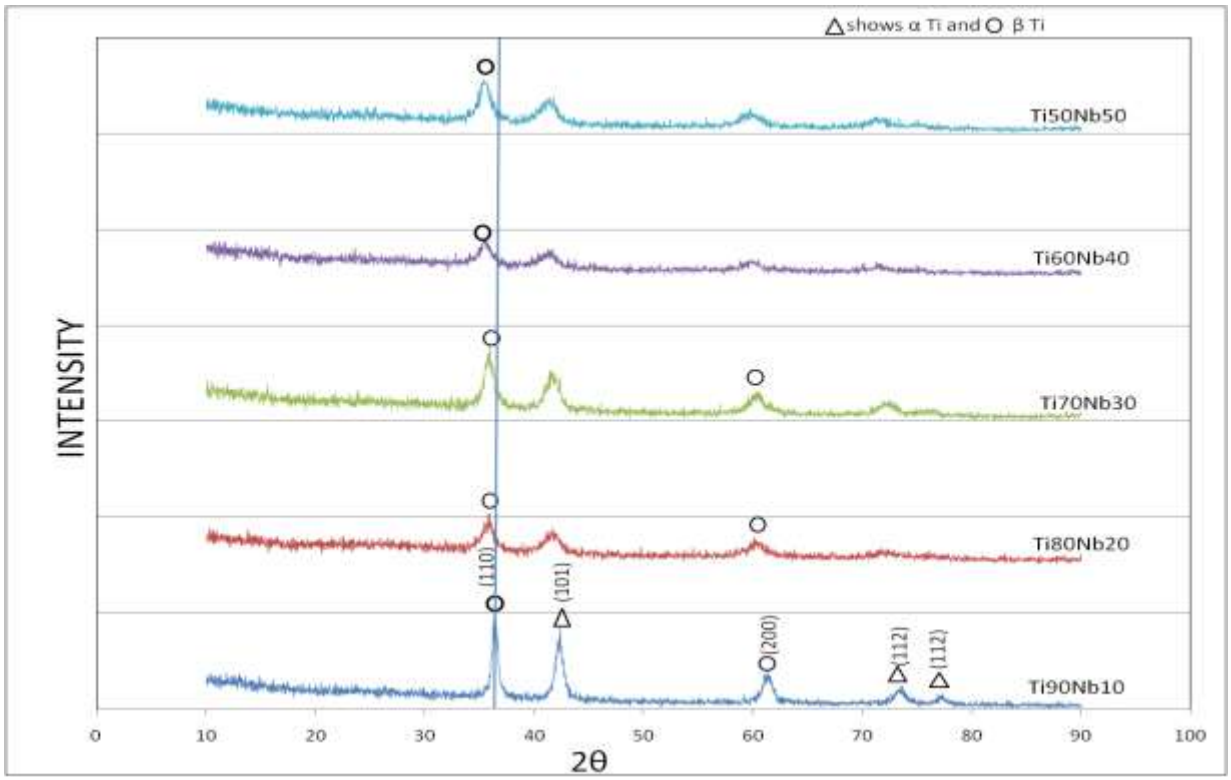

Figure 1. XRD diffraction pattern of Ti-Nb thin films

Prominent peak (110) of this alloy which is observed at angle 36.31° is found to shift to low 2θ, with the increase of niobium content, probably due to the intake of relatively bigger ion of Nb in Ti matrix. The 2nd highest peak due to (101) reflection observed at 42.3° only in Ti90Nb10 is due to α-phase. This peak becomes weak, broadened and finally disappears in case of Ti80Nb20 sample. The 3rd peak (200), observed at around 60° which is corresponding to β- phase becomes very weak after Ti70Nb30 indicating a reduction in the content of β- phase beyond replacement of Ti by Nb by more than 30%. The other two peaks (112) at around 73° and (112) at around 77° belonging to α- phase, virtually diminish after 10% replacement of Ti by Nb. Obviously, at 10% Nb, both α and β peaks are present. As niobium content increases, primary α- peak diminishes gradually; implying that original α-phase dominated structure gradually transforms into β- phase dominated structure. For 30% Nb, the α-

phase peaks completely disappear and only one β- peak (110) remains. The retention of β phase in Ti-Nb alloy at higher Nb content is consistent with the results of other investigations.[9]

Another interesting feature in XRD profiles of Ti-Nb alloy peaks are shifted towards lower angles. Shifting in peaks is due to increase in d-spacing. Increase in d-spacing is due to difference in ionic radii of Ti and Nb ions. The ionic radii of Nb ions is greater than Ti ions (Ti= 74.5pm and Nb=78pm). Increase in plane spacing (d values) is due to rearrangement of lattice positions. Hence it implies that 2θ shifts to lower values and lattice volume increases, suggesting that Nb ions are being incorporated into lattice. Relative values of peak intensities are closely related the contents of alloying element, however, the broadening of peaks may be attributed to increasing Nb concentration in alloys which in turn modifies the film texture also. Changes in film texture can be explained by interactions between the species involved in process. During film growth, the surface is bombarded by different high energy species of plasma. The magnitude of this bombardment depends on quantity and mass of species that form the film. Since Nb has higher atomic weight compared to Ti, the increase in Nb content causes an increase in number of species and total mass of metallic atoms in plasma, which may result in change in flux of species and energies with which species impact the surface and therefore may result in changes of film texture. To further look into this aspect, we calculated the average crystallite size by Scherrer formula.

$$Dp = (0.9 \times \lambda)/ (\beta \cos\theta) \qquad (1)$$

where Dp = Average Crystalline size, β = FWHM in radians, θ = Bragg angle, λ = X-Ray wavelength

Table 2 below summarizes our findings. Clearly, the crystallite size increases up to 20% substitution of Ti by Nb i.e. sample Ti80Nb20 and there after it starts decreasing as Nb content increases. The lattice strain is found to increases with decrease in crystallite size as shown in Table 2, which indicates a lower number of lattice imperfections. This may be due to a decrease in the occurrence of grain boundaries, thereby confirming the higher values of grain size.

Table 2: Crystallite Size, Lattice Strain and Other XRD Parameters for Ti-Nb Alloy Samples

Target Composition	XRD Peak Position [°2θ]	FWHM (radians)	Crystalline size (nm)	Intensity	d-spacing [Å]	Lattice Strain(10^{-3})
Ti90Nb10	36.3160	0.5904	14.80	146.78	2.47	7.9
Ti80Nb20	35.9113	0.4723	18.48	57.30	2.50	6.4
Ti70Nb30	35.7323	0.7085	12.31	98.70	2.51	9.6
Ti60Nb40	35.4057	0.7200	12.10	49.44	2.53	9.8
Ti50Nb50	35.4312	0.8640	10.09	77.84	2.53	11.8

The AFM images depicting the morphology of Ti-Nb films deposited on glass substrates at varying percentage of niobium are shown in Fig. 2 (a - e) with (i) and (ii) indicating the 2D and 3D images of the respective samples. Images of alloy were taken in 5µm x 5µm area. Light brown color shows the Titanium and white color indicates Niobium. Evidently, with an increase in niobium content, more white spots can be seen in the recorded images. The micro structural analysis showed an acicular microstructure growing with the increase of the niobium content. These niobium particles act as β-phase nucleation agent. With increasing Nb content, the increase of niobium particles continues with consequent increase in its volume fraction in the two-phase .

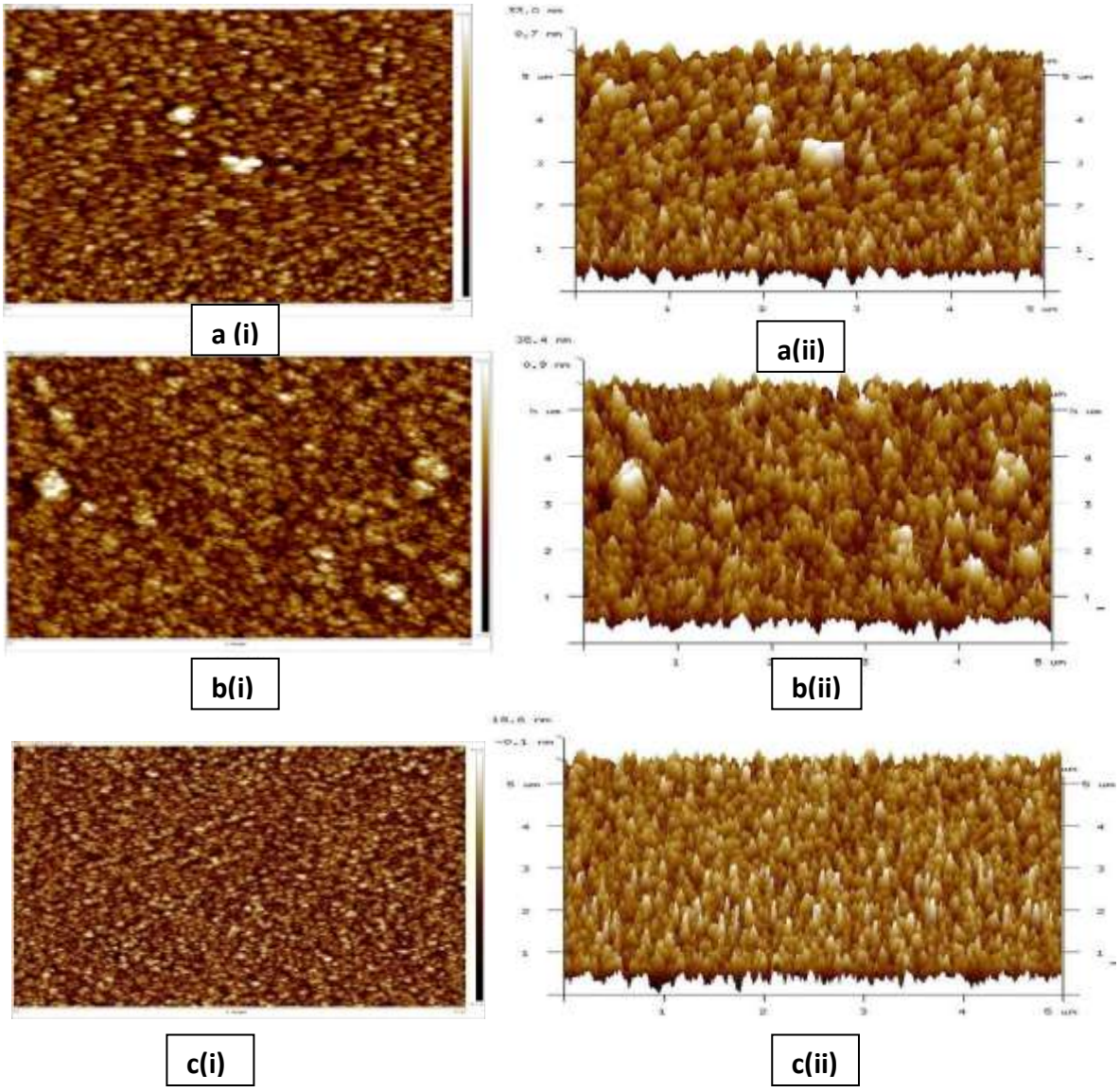

Cont.

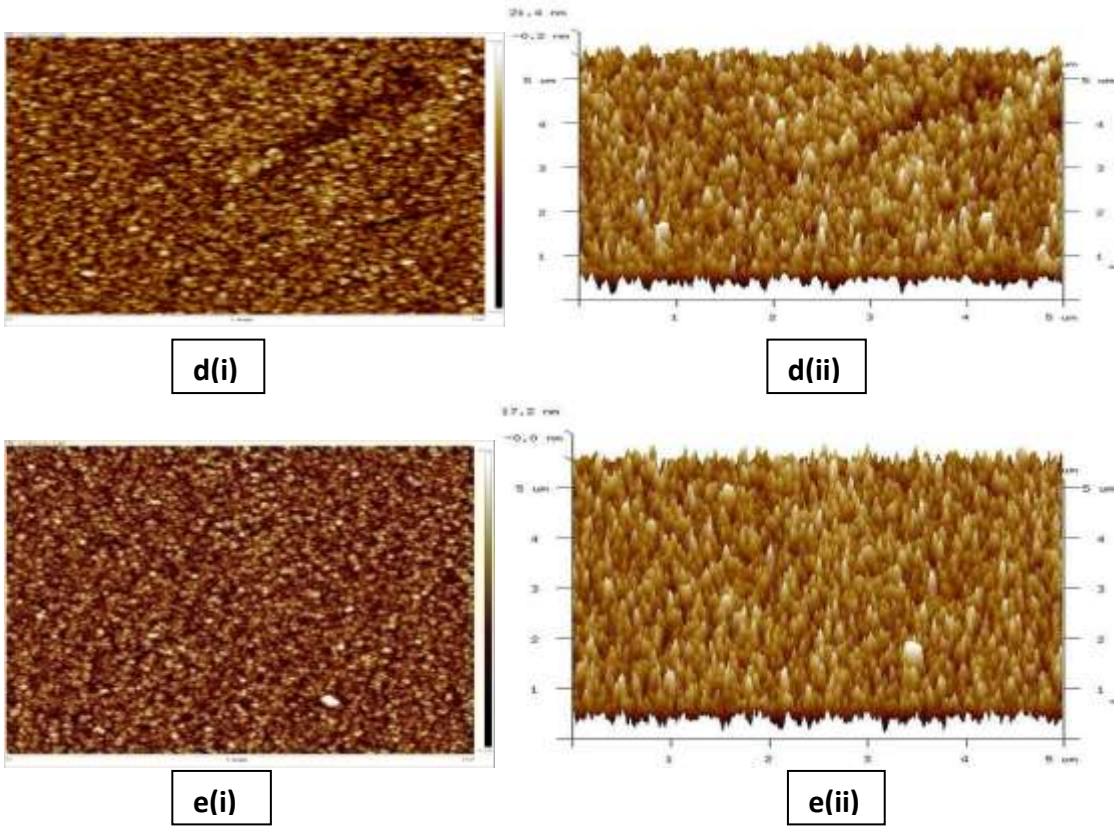

Figure 2: AFM images Ti-Nb films on glass substrate of different compositions a(i) 2D, a(ii) 3D of Ti90Nb10, b(i) 2D, b(ii) 3D of Ti80Nb20, c(i)2D, c(ii) 3D of Ti70Nb30, d(i) 2D, d(ii) 3D of Ti60Nb40, e(i) 2D, e(ii) 3D of Ti50Nb50

Structure and Nb particles reach more and more to the titanium rich areas. Clearly, these results show a more compact microstructure with continuously reducing porosity. At Ti50Nb50, most homogeneous microstructure with least porosity is obtained.

To further look into the surface characteristics of the synthesized samples, we have calculated the roughness using the AFM data. The roughness can be analytically described by various roughness parameters. Each sample was analyzed at five randomly chosen locations. Different parameters of roughness of all five samples for scanning areas of 2µm x 2µm and 5µm x 5µm are listed in Table 3 and Table 4 respectively. Clearly, the roughness parameter Ra decreases from 7.87 nm to 3.85 nm for 2µm x 2µm scanning area and from 7.14 nm to 3.95 nm for 5µm x 5µm area with the increase in Nb content. Another important roughness parameter Rq also decreases from 10.3 nm to 4.36 nm for 2µm x 2µm scanning area and from 9.23 nm to 4.96 nm for 5µm x 5µm scanning area. Therefore, as the content of niobium increases, roughness of the samples is found to decrease. This decrease in film roughness is due

to transformation of crystal structure of larger hexagonal grains, dominated by α-phase into β- phase with cubic symmetry, as evidenced from XRD studies. It is also visible in Fig. 2 that as the surface becomes smoother, the boundaries of grains come together, resulting into reduced porosity and enhanced compaction.

Table 3: Results of different parameters of roughness of AFM images at 2µm x 2µm

Alloy composition/ Results	Image Rq	Image Ra	Image Rmax	Rz	Rp
Ti90Nb10	10.3nm	7.87nm	118nm	147nm	73.4nm
Ti80Nb20	8.95nm	7.07nm	89.8nm	103nm	51.3nm
Ti70Nb30	5.34nm	4.24nm	45.4nm	52.1nm	26.1nm
Ti60Nb40	5.56nm	4.44nm	46.9nm	55.3nm	27.7nm
Ti50Nb50	4.86nm	3.85nm	42.2nm	48.5nm	24.2nm

Table 4: Results of different parameters of roughness of AFM images at 5µm x 5µm

Alloy composition/ Results	Image Rq	Image Ra	Image Rmax	Rz	Rp
Ti90Nb10	9.23nm	7.14nm	130nm	181nm	90.5nm
Ti80Nb20	9.56nm	7.53nm	98.7nm	111nm	55.6nm
Ti70Nb30	5.40nm	4.28nm	62nm	75.4nm	37.7nm
Ti60Nb40	6.16nm	4.77nm	70.1nm	70.9nm	35.5nm
Ti50Nb50	4.96nm	3.95nm	51.9nm	60.1nm	30.1nm

In order to further look into the microstructural features of the samples synthesized, we have recorded the FESEM micrographs of all the samples as shown in Fig. 3 (a - e) with (i) and (ii) indicating the 50k magnification and 200k magnification of images of the respective samples. Micro structural examination shows that, significant amount of β-phase present in all samples. These findings are in agreement with the results of XRD. In order to identify various phases present in the recorded micrographs, we have performed Energy Dispersive X-Ray Microanalysis (EDX) on these samples. Fig. 4(a-e) and Table 5 show the result of these investigations.

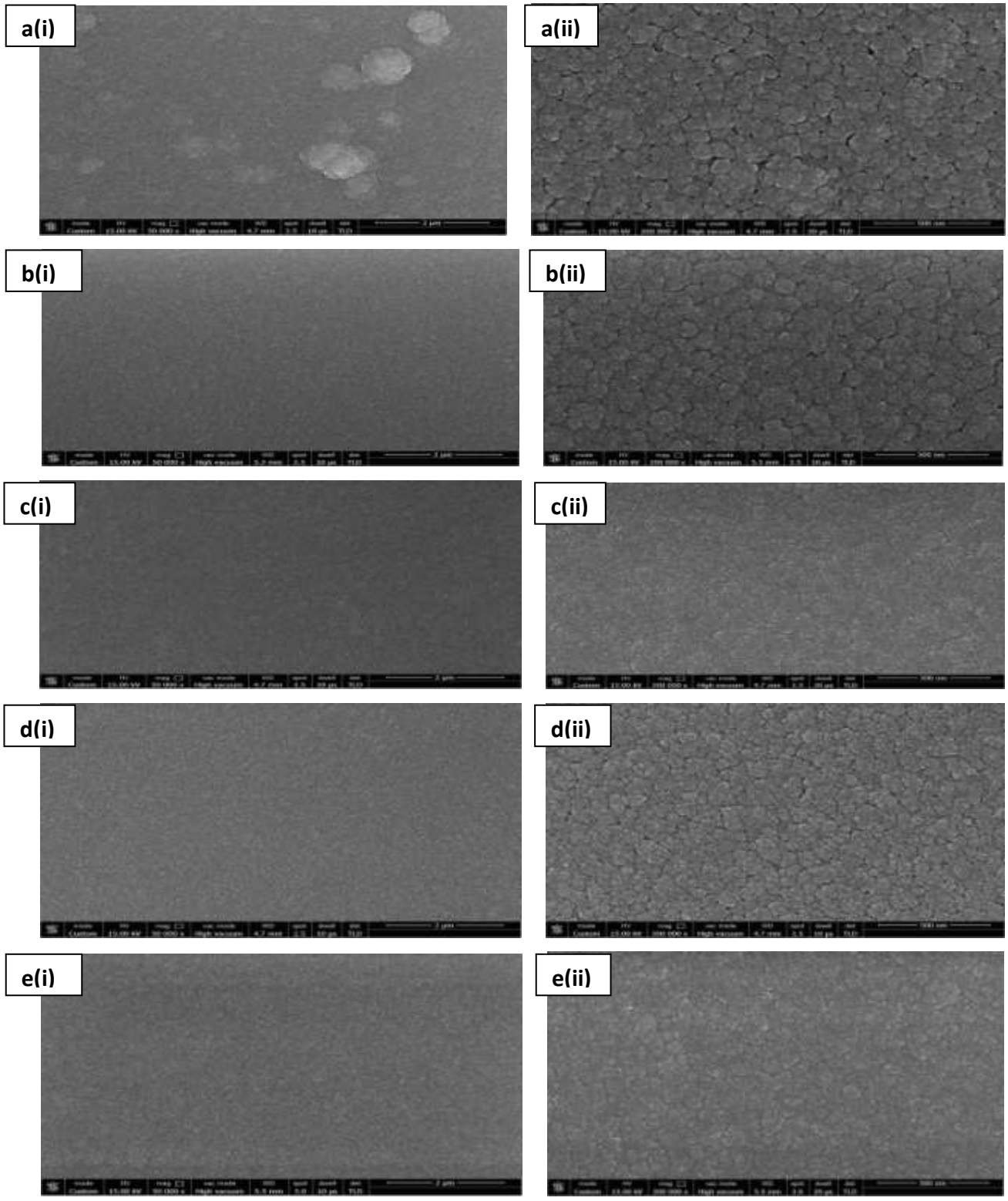

Figure 3: SEM images of Ti-Nb alloys at different magnification a(i) 50k, a(ii) 200k ofTi90Nb10, b(i) 50k, b(ii) 200k of Ti80Nb20, c(i) 50k, c(ii) 200k of Ti70Nb30, d(i) 50k, d(ii) 200k of Ti60Nb40, e(i) 50k, e(ii) 200k of Ti50Nb50

The Nb particles are found to be of white color and Ti particles are of dark grey color in the micrographs. Clearly with the increase in Nb content, more and more white spots are visible in the micrographs. The study of chemical composition of all the samples i.e. the Ti and Nb percentages validate the compositions of samples.

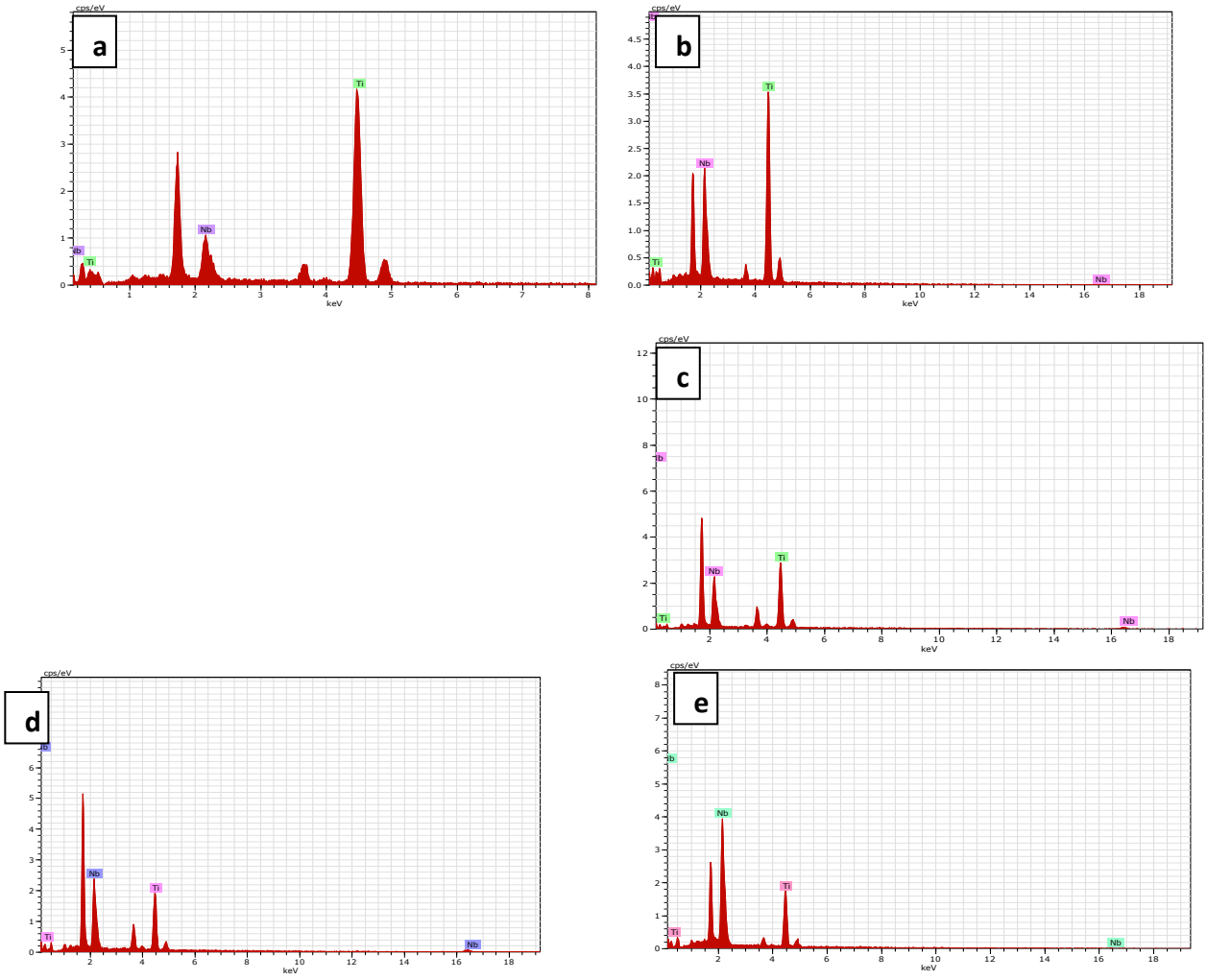

Fig. 4: EDX Patterns for Nb-Ti Alloy Samples (a) Ti90Nb10, (b) Ti80Nb20, (c) Ti70Nb30, (d) Ti60Nb40, (e) Ti50Nb50

The grain sizes of all these samples were calculated from online software Image J with images of 200k magnification. The Table 6 below shows the values of grain size as a function of sample composition. Clearly, with an increase in Nb content the grain size increases from 23 nm to 28 nm with an exception of Ti60Nb40 sample which is found to have excessively large grain size of 37 nm. The increase of grain size is found to be accompanied by a decrease in the film roughness as observed in AFM studies. Roughness arises from boundaries between grains, the more number of grains the more boundaries which means more roughness. Increased grain size means reduced number of grains and

therefore fewer boundaries and hence low value of roughness. As a general observation, all the samples are found to have uniform distribution of nano-grains and as Nb content increases from 10% to 50%, the size of the grains increases and surface becomes smoother and compact.

Table 5: EDX Chemical Analysis of all 05 Nb-Ti Alloy Samples

S.No	Target	Element	Series	Atomic Number	Weight %	At%	Error wt%
1.	Ti90Nb10	Ti	K-Series	22	82.05	89.87	1.69
		Nb	L-Series	41	17.95	10.13	0.55
2.	Ti80Nb20	Ti	K-Series	22	70.04	81.94	1.47
		Nb	L-Series	41	29.96	18.06	0.85
3.	Ti70Nb30	Ti	K-Series	22	54.27	67.18	1.05
		Nb	K-Series	41	45.73	32.82	0.48
4.	Ti60Nb40	Ti	K-Series	22	43.82	58.88	0.86
		Nb	K-Series	41	56.18	41.12	1.42
5.	Ti50Nb50	Ti	K-Series	22	33.45	49.38	0.65
		Nb	K-Series	41	66.55	50.62	2.25

Table 6: Grain size of Ti-Nb alloy

Sample composition	Ti90Nb10	Ti80Nb20	Ti70Nb30	Ti60Nb40	Ti50Nb50
Grain size (in nm)	23	17	26	37	28

It can further be noticed that an increase in Nb content led to increased homogeneity of distribution of Ti and Nb on SEM images. Density of films has increased with lesser fraction of voids. It is evident that with the increase in Nb content, the morphology of the grain changes and becomes denser due to higher surface and bulk diffusivity of sputtered atoms. Grains are found to size in nano- regime with regular shape, indicating good nano-crystallinity.

CONCLUSION:

The fine grained (Ti-Nb) alloys with nominal compositions $Ti_{90}Nb_{10}$ (Ti-17.7 wt.% Nb), $Ti_{80}Nb_{20}$ (Ti-33 wt.% Nb), $Ti_{70}Nb_{30}$ (Ti 45 wt.% Nb), $Ti_{60}Nb_{40}$ (Ti- 56 wt.% Nb) and $Ti_{50}Nb_{50}$ (Ti-66 wt.% Nb) were successfully prepared by RF sputtering method at relatively low temperature (200°C). Experimental results indicated that microstructure properties of Ti-Nb alloys are sensitive to Nb content. Increased Nb content changes the microstructure making more dense and compact. XRD results exhibited a shift in peaks towards low 2θ values indicating a solid state transformation from hexagonal to cubic symmetry. Both α- and β- phases were found to coexist in all the Nb-Ti alloy samples synthesized,. Increased addition of Nb had a direct effect on their growth modes. FESEM images of the films showed a uniform and dense morphology of alloy films in case of samples with higher Nb content.

The average grain size is found to increase from 23 nm ($Ti_{90}Nb_{10}$) to 28 nm ($Ti_{50}Nb_{50}$). The AFM and FESEM Images showed that samples were adequate homogeneous material. The films are found to show a decreasing trend in roughness with increasing Nb content. Average roughness is found to decrease from 7.87 nm ($Ti_{90}Nb_{10}$) to 3.85nm ($Ti_{50}Nb_{50}$) for 2µm x 2µm scanning area. Decrease in surface roughness of alloy is attributed to the smoother surface, reduced grain boundaries and transformation in crystal symmetry together with the increased grain size.

CONFLICT OF INTEREST: None

ACKNOWLEDGEMENT

: Authors acknowledge to all those who directly or indirectly contributed in this work.

REFERENCES

1. Kim HY, Sasaki T, Okutsu K, Kim JI, Inamura T, Hosoda H, Miyazaki S. Texture and shape memory behavior of Ti–22Nb–6Ta alloy. Acta Materialia. 2006 Jan 1; 54(2):423-33.

2. Tane M, Akita S, Nakano T, Hagihara K, Umakoshi Y, Niinomi M, Nakajima H. Peculiar elastic behavior of Ti–Nb–Ta–Zr single crystals. Acta Materialia. 2008 Jul 1;56(12):2856-63.

3. Hu QM, Li SJ, Hao YL, Yang R, Johansson B, Vitos L. Phase stability and elastic modulus of Ti alloys containing Nb, Zr, and/or Sn from first-principles calculations. Applied Physics Letters. 2008 Sep 22;93(12):121902.

4. Li SJ, Cui TC, Hao YL, Yang R. Fatigue properties of a metastable β-type titanium alloy with reversible phase transformation. Acta biomaterialia. 2008 Mar 1;4(2):305-17.

5. Hon YH, Wang JY, Pan YN. Composition/phase structure and properties of titanium-niobium alloys. Materials Transactions. 2003;44(11):2384-90.

6. Achache S, Lamri S, Yazdi MA, Billard A, François M, Sanchette F. Ni-free superelastic binary Ti–Nb coatings obtained by DC magnetron co-sputtering. Surface and Coatings Technology. 2015 Aug 15;275:283-8.

7. File PD. Joint committee on powder diffraction standards. ASTM, Philadelphia, Pa. 1967:9-185.

8. Han MK, Kim JY, Hwang MJ, Song HJ, Park YJ. Effect of Nb on the microstructure, mechanical properties, corrosion behavior, and cytotoxicity of Ti-Nb alloys. Materials. 2015 Sep 9;8(9):5986-6003.

9. Eylon D, Boyer RR, Koss DA. Minerals, Metals and Materials Society. 1st ed. Denver CO: United States; 1993; 25(12): p.542.